AN INVESTIGATION OF A FREE JET AT LOW REYNOLDS NUMBERS

by

George C. Greene

A thesis presented

in partial fulfillment of the requirements

for the degree of

MASTER OF ENGINEERING

Department of Mechanical Engineering
Old Dominion University
August 1973

Supervisory Committee

Donald F. Boltz
(Thesis Director)

Robert L. Ash

Surendra N. Tiwari

ABSTRACT

This thesis presents a comparison of the measured and calculated flow field properties of a nozzle of unusual design which was used to produce an incompressible, low Reynolds number jet. The "nozzle" is essentially a porous metal plate which covers the end of a pipe. Results are presented for nozzle Reynolds numbers from 50 to 1000 with velocities of 100 or 200 ft/sec. The nozzle produces a uniform velocity profile at nozzle Reynolds numbers well below those at which conventional contoured nozzles are completely filled with the boundary layer. A jet mixing analysis based on the boundary layer equations accurately predicted the flow field over the entire range of Reynolds numbers tested.

TABLE OF CONTENTS

ACKNOWLEDGEMENTS

The author would like to express his appreciation to the management of the Langley Research Center, NASA, for providing the facilities and financial support for this thesis. The author would also like to thank Dr. Donald F. Brink for his guidance, encouragement, and assistance during the preparation of this thesis.

LIST OF FIGURES AND TABLES

Page

Figure

Table

LIST OF SYMBOLS

c_p	specific heat at constant pressure
D	impact tube diameter
$\mathcal{D}$	diffusion coefficient
k	impact tube viscous correction constant
K	thermal conductivity
M	Mach number
p	pressure
R	nozzle radius
Re	Reynolds number based on diameter
S_i	mass concentration of i'th gas
T	temperature
u	velocity in the x direction
v	velocity in the y direction
v_{max}	maximum nozzle velocity at a given value of x/R
x,y,z	nozzle coordinates
γ	ratio of specific heats
ρ	density
μ	coefficient of viscosity
ζ,τ	coordinates in the modifided Von Mises plane

Subscripts

e	conditions at $y = \infty$
0	conditions at $x = 0$
T	stagnation conditions

∞	freestream conditions
i	impact tube conditions

INTRODUCTION

In the past decade several methods of measuring the temperature of the earth's upper atmosphere have been developed. In one of these methods a small sounding rocket is used to carry an instrument package and parachute aloft. The instrument package descends through the atmosphere suspended beneath the parachute and telemeters temperature data to the ground. Due to the low atmospheric density, the temperature transducer has a low degree of convective coupling to the atmosphere. Solar radiation represents a significant portion of the total heat transfer which results in degraded accuracy. In addition the recovery factor must be known in order to correct for aerodynamic heating. Therefore interpretation of the data requires calibration on the ground with flow conditions equivalent to those experienced in the upper atmosphere.

In a typical calibration arrangement, the temperature transducer is placed in a wind tunnel or jet of air to simulate the fall through the atmosphere. The flow Mach number and Reynolds number are duplicated to maintain the proper heat transfer characteristics. However, for very low Reynolds numbers, which are required to duplicate the conditions in the upper atmosphere, conventional wind tunnel nozzles develop very thick boundary layers. This problem becomes serious at nozzle Reynolds numbers of about 1000 and gets progressively worse until the entire nozzle is filled with the boundary layer at Reynolds numbers of about 200 [1].

Due to this Reynolds number limitation, a small research program was initiated to develop a low Reynolds number nozzle for a calibration facility at the Langley Research Center. A literature search revealed that a multi-jet nozzle was a potential solution to the large boundary layer problem. In a multi-jet nozzle the flow is broken down into a number of small jets which combine through viscous interaction to form a uniform flow downstream of the nozzle. A supersonic multi-jet nozzle (consisting of 37 holes in a 2 inch diameter steel plate) was tested at Ames Research Center with only partial success [1]. Although the nozzle did produce a uniform velocity profile, the flow was not established until it had gone many diameters downstream.

The nozzle used in the present study is an extension of this concept to a large number of very small jets. With very small jets, local viscous interaction is much greater and a uniform flow is established almost immediately downstream of the nozzle. Since it did not seem feasible to accurately drill a large number of small holes, a number of naturally porous materials were tested on a trial and error basis. The first materials tested were paper filters with various porosities. All of these exhibited large deflections at high flow rates which tended to distort the velocity profile. The addition of copper reinforcing screens produced adequate nozzle performance except at very high flow rates. The nozzle material which finally evolved consists entirely of stainless steel screens which were sintered to form a 1/8 inch thick plate. This was very rigid

and produced a reasonably uniform velocity profile over a wide range of flowrates.

The purpose of this thesis is to describe the performance characteristics of this nozzle for nozzle Reynolds numbers between 50 and 1000 and to compare the nozzle flowfield data with the calculated results of an incompressible boundary layer type analysis.

APPARATUS

Figure 1 shows a schematic diagram of the test apparatus used in this investigation. The porous plate nozzle was bolted to the end of a 7-5/8 inch diameter nozzle pipe which extended through the wall of a large (55 feet diameter) vacuum chamber. The porous plate nozzle was made of 5 layers of stainless steel screen which were sintered to form a rigid plate 1/8 inch thick. The innermost screen had a mesh size of about 5 microinches. The outer screens were of a larger mesh size for strength. The sintered screens are sold commercially by the Bendix Corporation, Filter Division under the brand name Poroplate.

Outside the vacuum chamber an air supply was passed through a dryer, pressure regulator, vertical tube flowmeter, and manual control valve into the nozzle pipe. The airstream stagnation temperature was measured inside the nozzle pipe using a shielded thermocouple. Downstream from the nozzle the flow Mach number was determined from measurements of the static pressure and the difference between the total and static pressures using the one-dimensional isentropic flow equations.

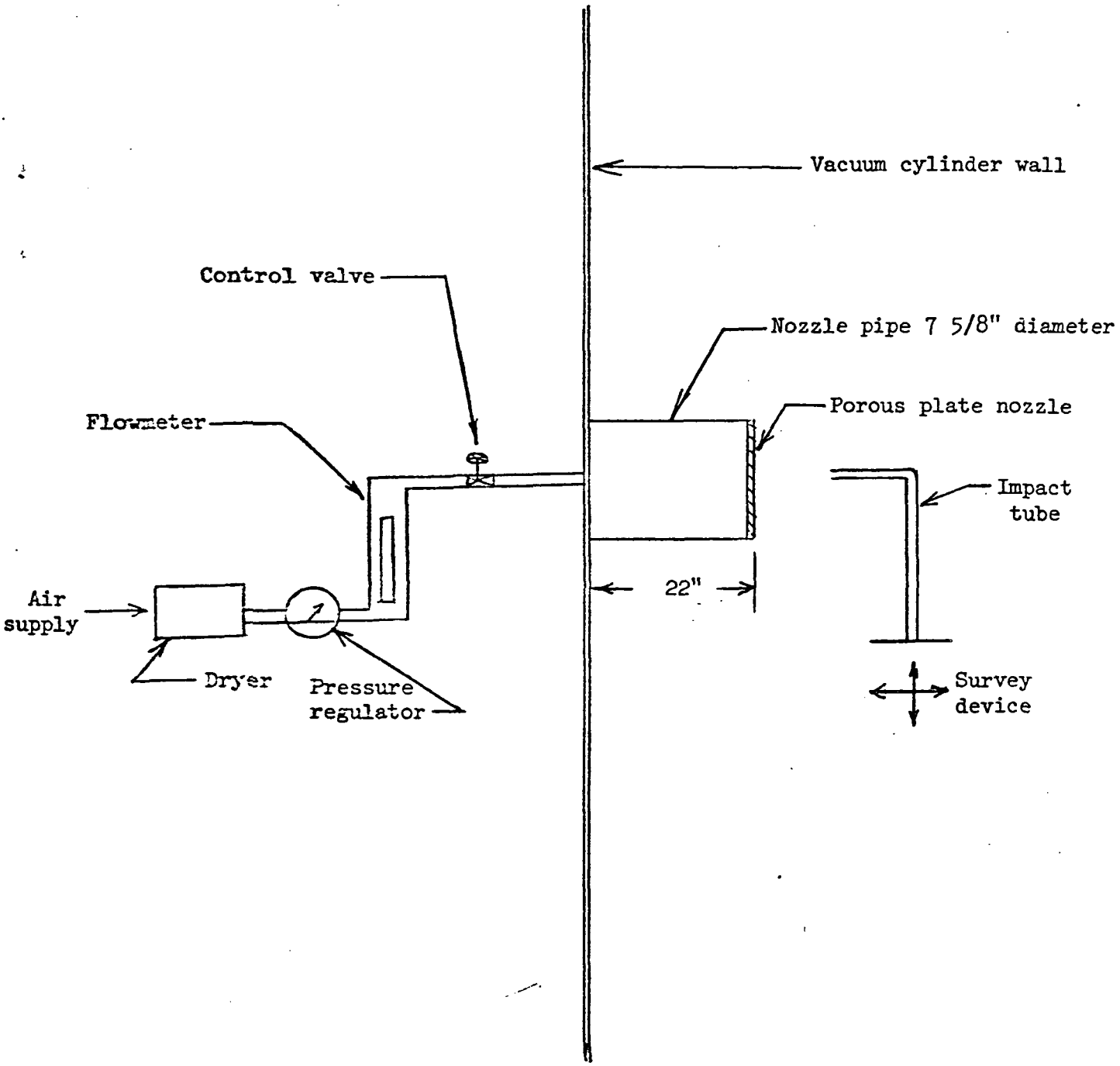

Figure 1.- Schematic diagram of test apparatus.

The total pressure was determined from impact tube measurements after applying a viscous correction. This correction is described in detail in the section entitled "Impact Tube Viscous Corrections." A Baratron differential pressure transducer with a range zero to 10 torr was used to measure the difference between the impact tube pressure and the static pressure. The static pressure throughout the jet was assumed to be the same as the background gas pressure since the flow was subsonic. The background pressure was measured at a point near the nozzle using a Baratron absolute pressure transducer with a range zero to 10 torr. Both pressure transducers were kept in a controlled temperature environment to minimize temperature effects.

The flowfield surveys were made by moving the impact tube with a two-dimensional survey device. The survey device was constructed and aligned so that surveys could be made either axially along the nozzle centerline or vertically along a nozzle radius. Calibrated potentiometers were used to indicate the distance in each survey direction.

All position, pressure, and temperature data were recorded on a Vidar digital data acquisition system. This system recorded at a rate of 40 data channels per second and produced either magnetic tape, printed output or both.

IMPACT TUBE VISCOUS CORRECTIONS

In this study the flow Mach number was determined from the total and static pressures using the isentropic flow equations. The total

pressure was obtained from impact tube measurements after applying viscous corrections. The impact tube used in this study is shown schematically in Figure 2. It was constructed to duplicate (as nearly as possible) a probe described by Sherman [2]. In [2], several probes were calibrated to determine the magnitude of the errors resulting from viscous flow about the probes at low Reynolds numbers.

A discussion of impact tube errors at low Reynolds numbers and an analytical solution for certain types of probes is given by Schaaf [3]. For a probe pointing into the gas stream, a boundary layer forms at the stagnation point on the tip of the probe. Using the coordinate system shown in Figure 3, the y-component of the Navier-Stokes equations for incompressible flow along the stagnation streamline can be written in the following form

$$\rho v \frac{\partial v}{\partial y} = -\frac{\partial p}{\partial y} + \mu \frac{\partial^2 v}{\partial y^2} \qquad (1)$$

This equation can be integrated through the boundary layer to give

$$p_i = p_\infty + \rho U_\infty^2/2 - \mu \left(\frac{\partial v}{\partial y}\right)_{y=\delta} + \mu \left(\frac{\partial v}{\partial y}\right)_{y=0}, \qquad (2)$$

since the pressure and velocity at the outer edge of the boundary layer are the same as in the free stream. From the continuity equation and flow symmetry about the stagnation streamline, it follows that

$$\frac{\partial v}{\partial y} = -\frac{\partial u}{\partial x} - \frac{\partial w}{\partial z} = -2 \frac{\partial u}{\partial x} \qquad (3)$$

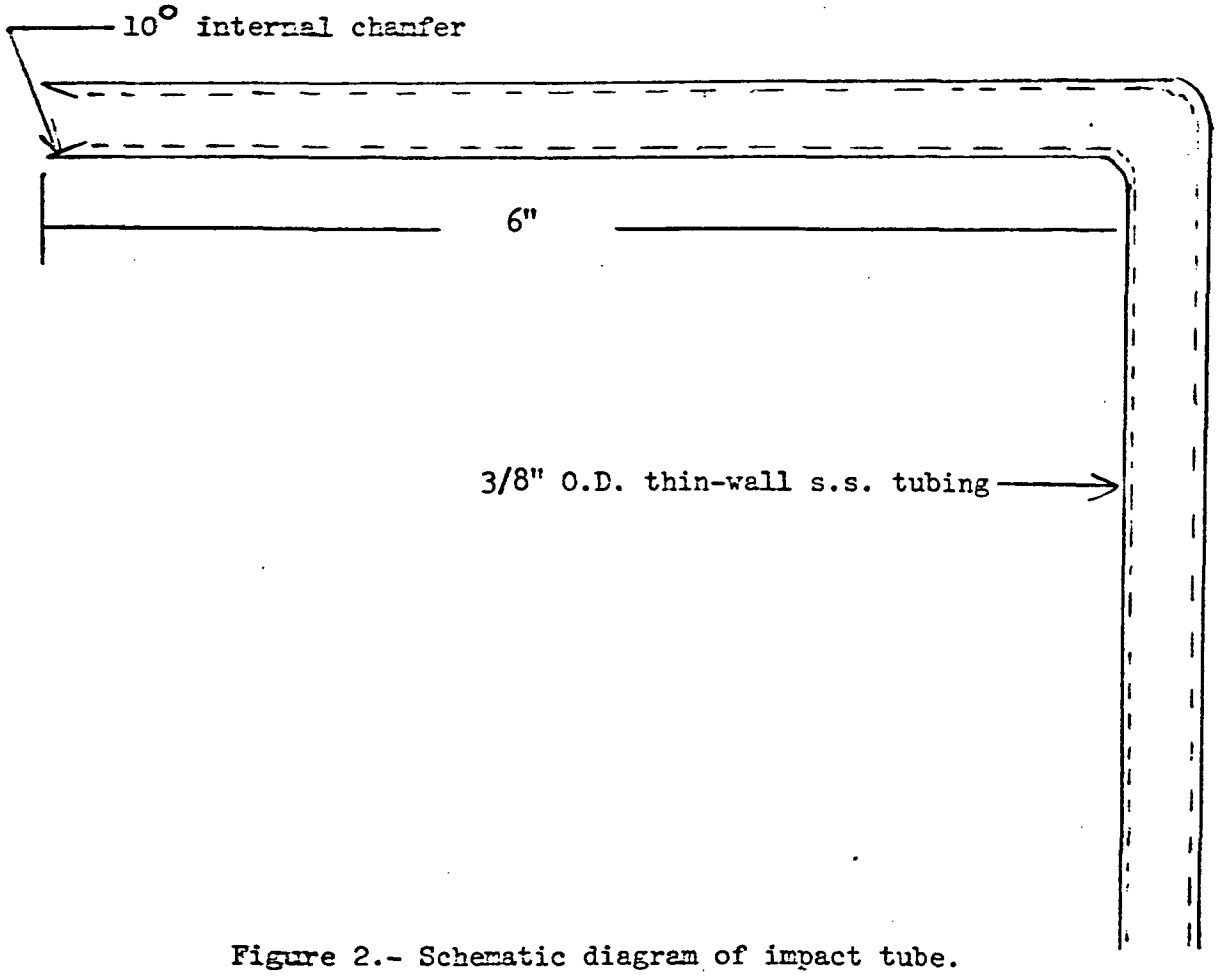

Figure 2.- Schematic diagram of impact tube.

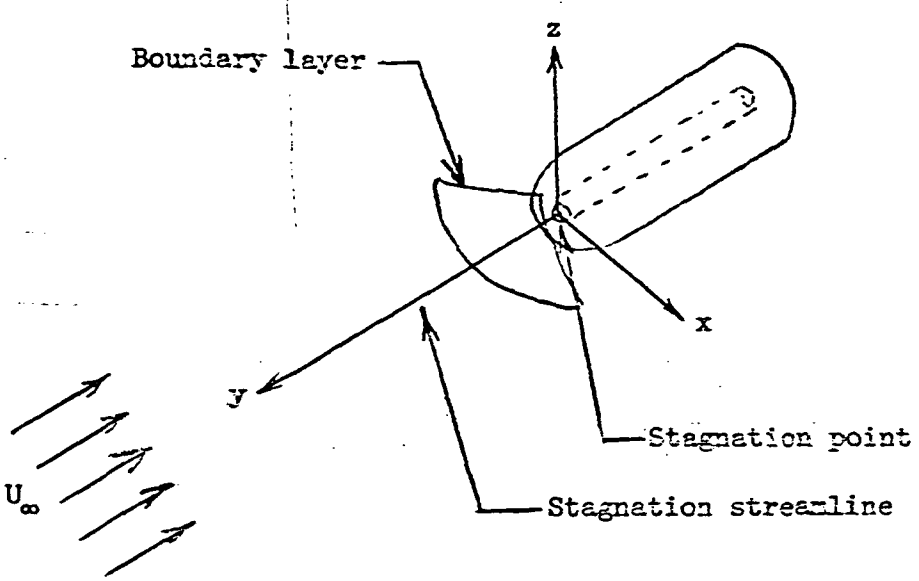

Figure 3.- Impact tube coordinate system.

As a result of the boundary condition at the wall $(\frac{\partial u}{\partial x})_{y = 0} = 0$, equation (3) yields

$$(\frac{\partial v}{\partial y})_{y = 0} = 0$$

Therefore equation (2) becomes

$$p_i = p_\infty + \rho U_\infty^2/2 + 2\mu (\frac{\partial u}{\partial x})_{y=\delta} \tag{4}$$

From a potential flow analysis the velocity gradient $(\frac{\partial u}{\partial x})_{y=\delta}$ can be determined analytically for simple shapes, such as a spherical tipped probe [4]. For a more complicated geometry such as the open-ended probe used in this study, $(\frac{\partial u}{\partial x})_{y=\delta}$ can be approximated by $k/4\ (u_\infty/D)$ where k is a constant which depends only on the probe geometry. The equation for impact pressure then has the form

$$P_i = P_\infty + \rho u_\infty^2/2 + k\mu u_\infty/2D \tag{5}$$

or

$$\frac{P_i - P_\infty}{\rho u_\infty^2/2} = 1 + \frac{k\mu}{\rho u_\infty D} = 1 + \frac{k}{Re} \tag{6}$$

Thus for large Reynolds numbers the correction term $\frac{k}{Re}$ is small and $p_i - p_\infty \approx \rho u_\infty^2/2$. When the Reynolds number becomes very small, $p_i - p_\infty$ becomes greater than $\rho u_\infty^2/2$.

As previously mentioned the constant, k, depends on the probe geometry, and must be determined experimentally. Since the probe used in this study was essentially a duplicate of one of the probes tested by Sherman [2], a value of k equal to 6, determined by fitting a curve through the data in Figure 5 of [2], was used.

Once the value of k is known, the flow velocity may be calculated as follows for incompressible flow:

$$P_i - P_\infty = \left(1 + \frac{k}{Re}\right)\left(\rho U_\infty^2/2\right) = \left(1 + \frac{k\mu}{\rho U_\infty D}\right)\left(\rho U_\infty^2/2\right) \tag{7}$$

By rearranging and dividing by $\rho/2$, the above equation becomes

$$U_\infty^2 + \frac{k\mu U_\infty}{\rho D} - \frac{2}{\rho}\left(P_i - P_\infty\right) = 0 \tag{8}$$

from which one can solve for the velocity as

$$U_\infty = -\frac{k\mu}{2\rho D} + \sqrt{\left(\frac{k\mu}{2\rho D}\right)^2 + 2\left(\frac{P_i - P_\infty}{\rho}\right)} \tag{9}$$

The values of ρ and μ in equation (9) are determined from the static temperature and pressure. Equation (9) therefore provides the corrected velocity in terms of the measured parameters.

TEST CONDITIONS AND PROCEDURE

Flowfield surveys were made at nozzle Reynolds numbers of 50, 100, 200, 600, and 1000. Nominal flow velocities were either 100

or 200 ft/sec. The resulting Mach numbers were approximately 0.089 and 0.178, respectively, which were sufficiently low to insure essentially incompressible flow conditions. The Reynolds number was varied by changing the density of the air. The flow conditions for each Reynolds number are listed in Table 1.

For testing at low pressures a continuous flow capability is highly desirable in order to allow sufficient run time to establish stable flow conditions and make the required measurements. In the present study continuous flow conditions were maintained for all nozzle flowrates.

Before each test the static pressure transducer was checked against a reference transducer to check for zero drift. The differential pressure transducer which was used to measure the impact tube pressure was checked for zero drift when the chamber was at the desired static pressure just prior to establishing the flow. The desired flow conditions were established based on the indicated dynamic pressure from the impact tube measurement with precomputed viscous corrections. Preliminary surveys were made to establish the fact that the jet was axisymmetric. Surveys were then made from the jet centerline outward along a radius at various positions along the jet axis. Survey data were recorded on the data acquisition system. After a complete flowfield survey, the process was repeated for the next Reynolds number.

TABLE 1. TEST CONDITIONS

Nozzle Reynolds Number	Static Pressure x 10^3 mmHg	Dynamic Pressure x 10^3 mmHg	$p_i - p_\infty$ x 10^3 mmHg	Nominal Velocity ft/sec
50	100	0.55	1.86	100
100	200	1.09	2.41	100
200	200	4.42	7.06	200
600	600	13.26	15.90	200
1000	1000	22.09	24.73	200

JET FLOWFIELD ANALYSIS

The jet flowfield was analyzed using the computer program described by Fox, Sinha and Weinberger [5]. The program has been adapted to the CDC 6000 series computer system and was used with only superficial modifications.

Basically the program solved the compressible, axisymmetric boundary layer equations in the Von Mises plane using an implicit finite difference numerical technique. Thus the applicable equations for the flow field sketched in Figure 4 are as follows:

Conservation of mass

$$\frac{\partial(\rho u y)}{\partial x} + \frac{\partial(\rho v y)}{\partial y} = 0 \tag{10}$$

Conservation of momentum

$$\rho u \frac{\partial u}{\partial x} + \rho v \frac{\partial u}{\partial y} = -\frac{\partial p}{\partial x} + \frac{\mu}{y}\frac{\partial u}{\partial y} + \mu \frac{\partial^2 u}{\partial y^2} \tag{11}$$

Conservation of energy

$$\rho u c_p \frac{\partial T}{\partial x} + \rho v c_p \frac{\partial T}{\partial y} = u\frac{\partial p}{\partial x} + K\frac{\partial^2 T}{\partial y^2} + \frac{K}{y}\frac{\partial T}{\partial y} + \mu\left(\frac{\partial u}{\partial y}\right)^2 + \rho \mathcal{D} \sum c_{p_i} \frac{\partial s_i}{\partial y}\left(\frac{\partial T}{\partial y}\right) \tag{12}$$

$$i = 1, 2$$

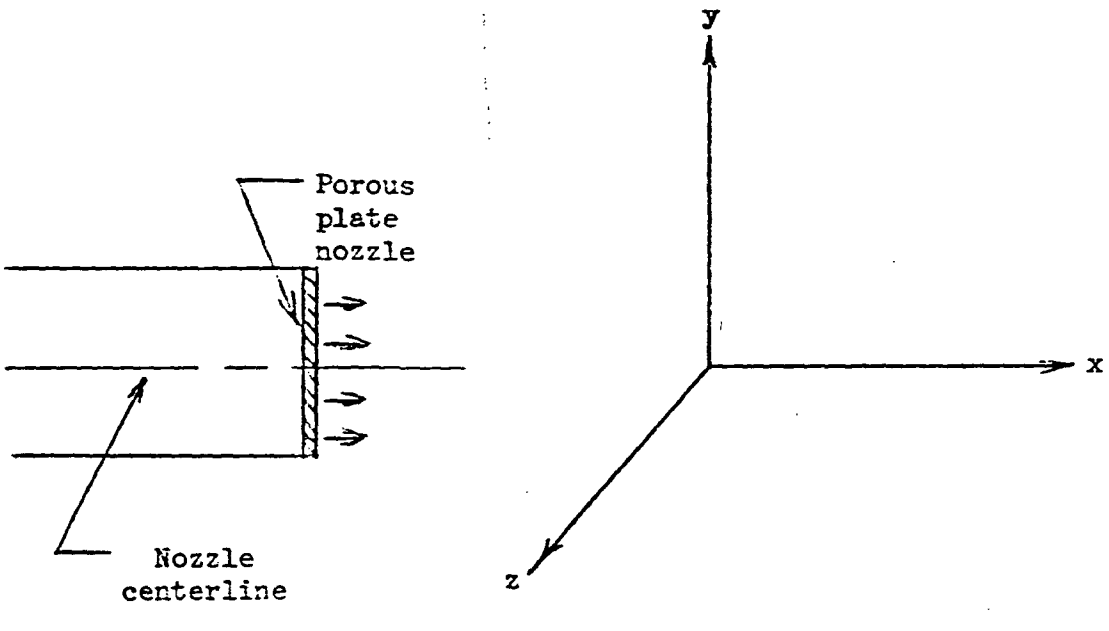

Figure 4.- Nozzle cooridnate system.

Conservation of species

$$\rho u \frac{\partial S_i}{\partial x} + \rho v \frac{\partial S_i}{\partial y} = \rho \mathcal{D} \frac{\partial^2 S_i}{\partial y^2} + \frac{\rho \mathcal{D}}{y} \frac{\partial S_i}{\partial y} \qquad (13)$$

$$i = 1, 2$$

Initially, the velocity, temperature, and gas concentrations are specified as:

$$\begin{aligned} u(x_0, y) &= u_0(y) \\ T(x_0, y) &= T_0(y) \\ S_i(x_0, y) &= S_{i_e}(y) \end{aligned} \qquad (14)$$

The boundary conditions at the center of the jet due to flow symmetry are

$$\frac{\partial u(x,0)}{\partial y} = \frac{\partial T(x,0)}{\partial y} = \frac{\partial S_i(x,0)}{\partial y} = 0 \qquad (15)$$

At the outer edge of the jet, one can write

$$\begin{aligned} \lim_{y \to \infty} u(x,y) &= u_e \\ \lim_{y \to \infty} T(x,y) &= T_e \\ \lim_{y \to \infty} S_i(x,y) &= S_{i_e} \end{aligned} \qquad (16)$$

By defining dimensionless quantities as

$$\bar{x} = x/R$$
$$\bar{y} = y/R$$

$$\begin{aligned} \bar{u} &= u / u_e \\ \bar{v} &= v / u_e \\ \bar{\rho} &= \rho / \rho_e \\ \bar{T} &= T / T_e \\ \bar{c}_p &= c_p / c_{p_e} \end{aligned} \tag{17}$$

the conservation equations can be solved in the modified Von Mises plane which is defined for axisymmetric flow by:

$$\xi = 1/4 \int_{\bar{x}_0}^{\bar{x}} \frac{d\bar{x}}{R_e} \tag{18}$$

and

$$\begin{aligned} 2\tau \frac{\partial \tau}{\partial y} &= \bar{\rho}\bar{u}\bar{y} \\ 2\tau \frac{\partial \tau}{\partial x} &= -\bar{\rho}\bar{u}\bar{y} \\ \tau &= \left(\int_0^{\bar{y}} \bar{\rho}\bar{u}\bar{y}\, d\bar{y} \right)^{1/2} \end{aligned} \tag{19}$$

It should be noted that since the edge conditions were used to normalize the velocities, the case of $u_e = 0$ cannot be solved. However, this is usually not a problem since u_e may be made very small, and was not zero in the actual experiment.

DATA ACCURACY

An error estimate was made for each of the variables of interest in this study. The errors in the measured quantities were determined directly from instrument characteristics. The errors in calculated quantities were based on the errors of each measured quantity which was used in the calculation. An error summary is presented in Table 2.

The mass flow and total temperature accuracies are based on the manufacturers' specifications for each instrument. Since the nozzle mass flow rate was used only for a qualitative check of the average nozzle velocity, an additional mass flow calibration did not appear to be justified. The $\pm 2^{\circ}F$ total temperature error represents only 0.4 percent of the absolute temperature and is a relatively small error source.

The error in both the static pressure and the difference between the impact tube and static pressure is primarily due to instrument zero drift. The static pressure transducer was located in a small controlled environment chamber inside the large vacuum chamber. The transducer was not readily accessible for zero calibration since this required physically pumping the transducer to zero pressure. However, a reference transducer which was calibrated against a secondary standard was kept pumped down to essentially zero pressure. Just prior to each test, the static pressure was measured using both transducers and the reading of the static pressure transducer corrected to the value indicated by the reference transducer. Zero check for

TABLE 2. DATA ACCURACY

Variable	Error Magnitude	Comments
$\dot{m}$	$\pm$.05 SCFM	Manufacturer's spec.
T_T	$\pm 2^{\circ}F$	Manufacturer's spec.
p_∞	$\pm 3 \times 10^{-3}$ mmHg	Short term accuracy
$p_i - p_\infty$	$\pm 1 \times 10^{-4}$ mmHg	Recalibrated for each test
x,y	$\pm$.03 inch	Primarily gear backlash
ρ	$\pm$0.7 to $\pm$3.4%	Based on temperature and pressure errors and perfect gas relation
μ	$\pm$0.3%	Based on temperature error and Sutherland viscosity equation
v	$\pm$1% to $\pm$7%	Based on pressure and temperature errors and 10% uncertainty in the impact tube viscous correction constant
Re	$\pm$2% to $\pm$11%	Based on errors in ρ, v, and μ

the differential pressure transducer was relatively easy. This was done just before each test before flow conditions were established.

The error in measuring the survey probe position was estimated to be about $\pm$.03 inch primarily due to gear backlash on the survey device. The error was estimated by clamping the probe in a fixed position and monitoring the position readout while turning the motor in either direction.

Table 2 also gives an error estimate for variables calculated from the primary measurements. The density error is based on a combination of the temperature and pressure errors through the perfect gas equation assuming that the gas constant is known. The viscosity error is based on the temperature error and the Sutherland viscosity equation given in [6].

The error in determining the flow velocity is based on a 10 percent uncertainty in the impact tube viscous correction constant, the temperature error for determining the speed of sound, and the pressure errors for determining the Mach number. The error in the speed of sound is only $\pm$0.2 percent assuming that the ratio of specific heats and gas constant are known. The Mach number error in terms of the pressure ratio error is given by

$$\frac{\delta M}{M} = \left[\frac{1+\left(\frac{\gamma-1}{2}\right)M^2}{\gamma M^2}\right] \frac{\delta\left(\frac{P_T}{P_\infty}\right)}{\left(\frac{P_T}{P_\infty}\right)} \qquad (20)$$

or in terms of the measured quantities

$$\frac{\delta M}{M} = \left[\frac{1+\left(\frac{\gamma-1}{2}\right)M^2}{\gamma M^2}\right]\left[1-\left(1+\frac{\gamma-1}{2}M^2\right)^{-\frac{\gamma}{\gamma-1}}\right]\left[\left|\frac{\delta P_\infty}{P_\infty}\right|+\left|\frac{\delta(P_T-P_\infty)}{P_T-P_\infty}\right|\right] \quad (21)$$

The velocity error is then the sum of the Mach number error and speed of sound error.

The error in Reynolds number is simply the sum of the errors in density, viscosity, and velocity. The error in measuring probe diameter is included in the uncertainty of the impact tube viscous correction constant.

RESULTS AND DISCUSSION

Figure 5 shows the development of the jet velocity profiles in the downstream direction for a nozzle Reynolds number of 1000. Velocity profiles are shown for three axial stations: x/R = 1, 2.5, and 7. For each velocity profile, the ratio of local velocity to the maximum jet velocity, v/v_{max}, was plotted against the non-dimensional radial coordinate, y/R. The symbols represent the measured data and the solid line represents the computed results. The measured and computed results are in good agreement, especially in the mixing region except at x/R = 7. As can be seen a very large potential core exists as far downstream as x/R = 7 which was the maximum distance for which measurements were taken. The calculated results indicate that the potential core would extend to about x/R = 30.

Figure 6 shows a set of velocity profiles for a nozzle Reynolds number of 600. Again, v/v_{max} is plotted against y/R for x/R = 1, 2.5, and 7.79. The agreement between calculated and measured

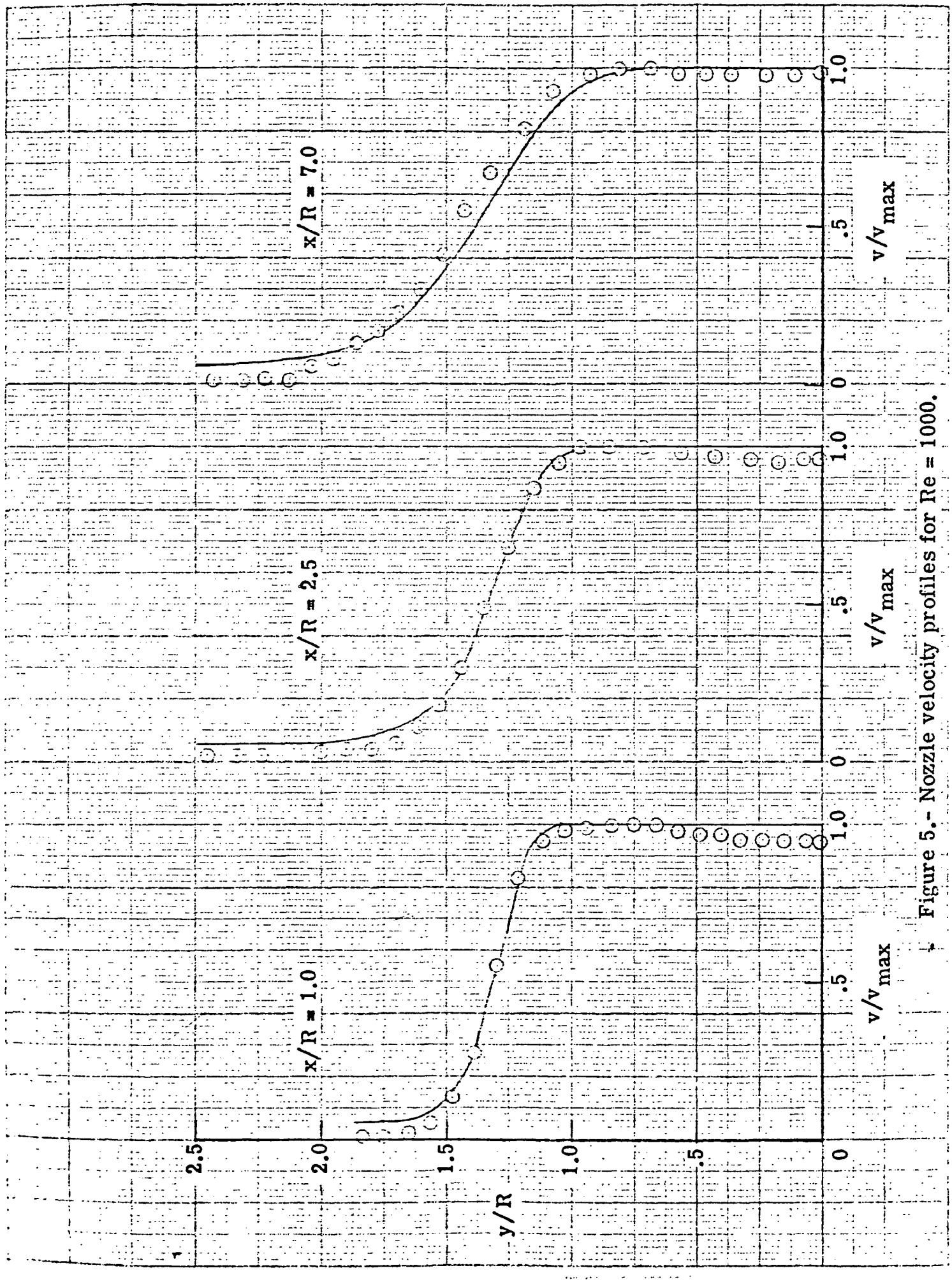

Figure 5.- Nozzle velocity profiles for Re = 1000.

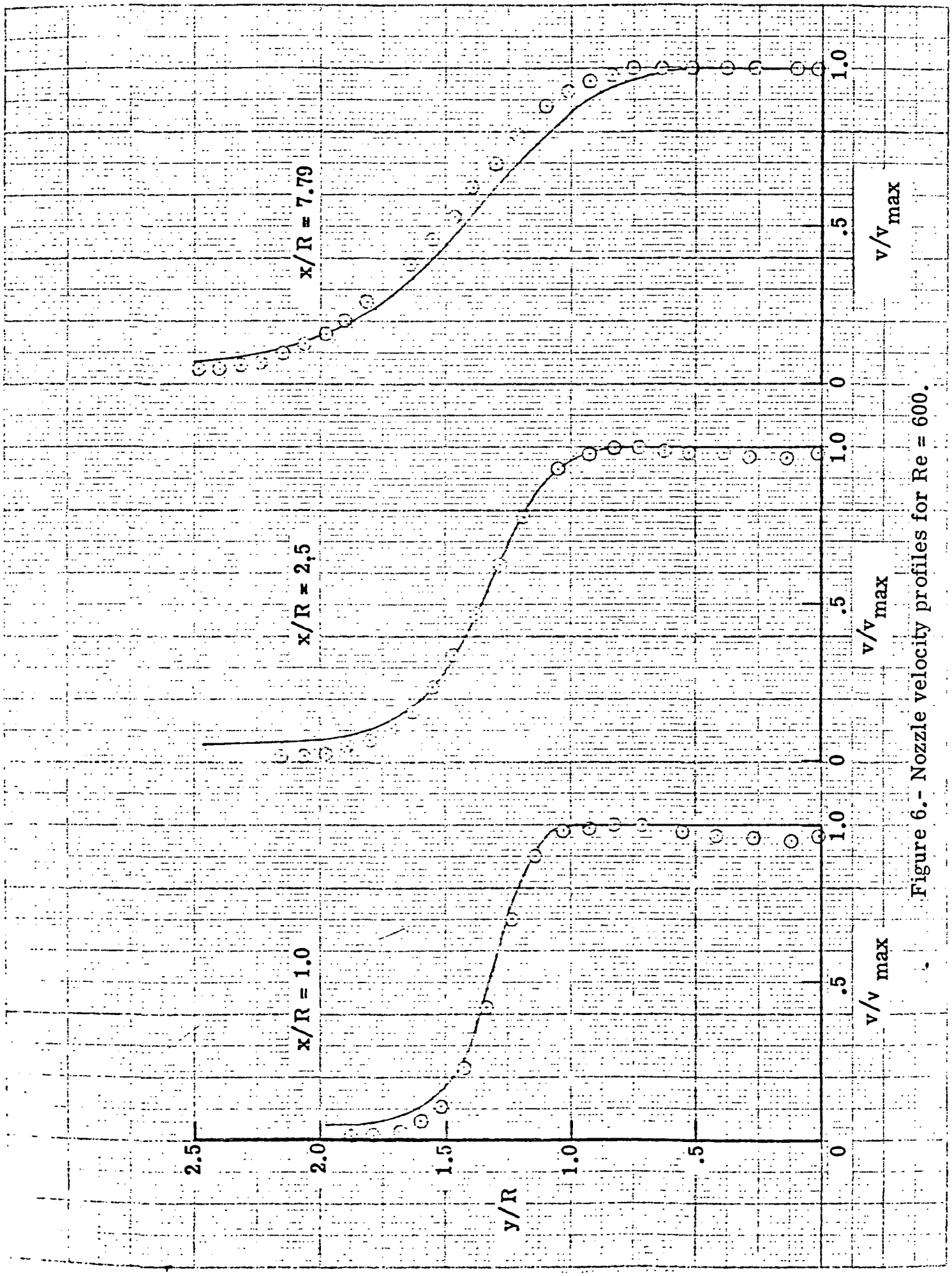

Figure 6.- Nozzle velocity profiles for Re = 600.

results is good except at 7.79. The potential core is still reasonably large at $x/R = 7.79$ and according to the analysis, it extended downstream to about $x/R = 20$.

Figure 7 shows typical velocity profiles for a nozzle Reynolds number of 200. v/v_{max} is plotted against y/R for $x/R = 0.5$, 2.5, and 6.0. The agreement between measured and calculated results is again very good. The potential core extends downstream to about $x/R = 6$. At $x/R = 0.5$ and 2.5, there is a reasonably large region of uniform velocity. It should be noted that at Reynolds numbers of about 200, a conventional contoured nozzle would be nearly filled with boundary layer at the nozzle exit.

Figure 8 shows the calculated and measured flow field data for a nozzle Reynolds number of 100. v/v_{max} is plotted against y/R for $x/R = 0.5$, 1.0, and 2.5. The potential core extends downstream just slightly beyond $x/R = 2.5$. At $x/R = 0.5$ and 1.0 there still remains a relatively large area of uniform flow.

Figure 9 shows the velocity profiles for a nozzle Reynolds number of 50, the lowest Reynolds number at which flow surveys were made. v/v_{max} is again plotted versus y/R for $x/R = 1.0$, 2.5, and 5.0. The potential core extends downstream to only about $x/R = 1.0$. The calculated results, which agree with the data very well further downstream, indicate that there is a large region of uniform flow just downstream of the nozzle. For example, at $x/R = 0.5$, the calculated results indicate that the potential core extends out radially to $y/R = 0.5$.

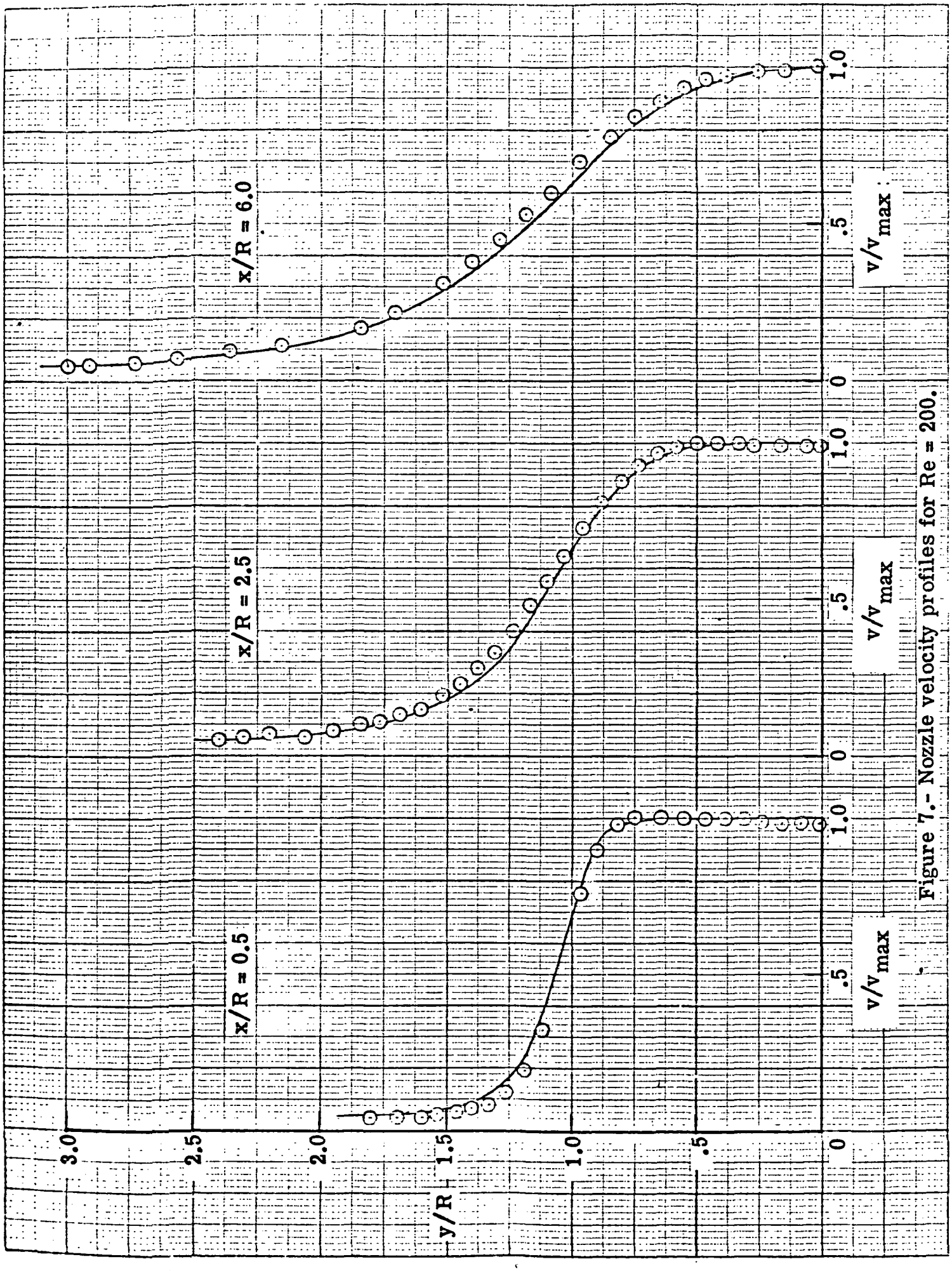

Figure 7.- Nozzle velocity profiles for Re = 200.

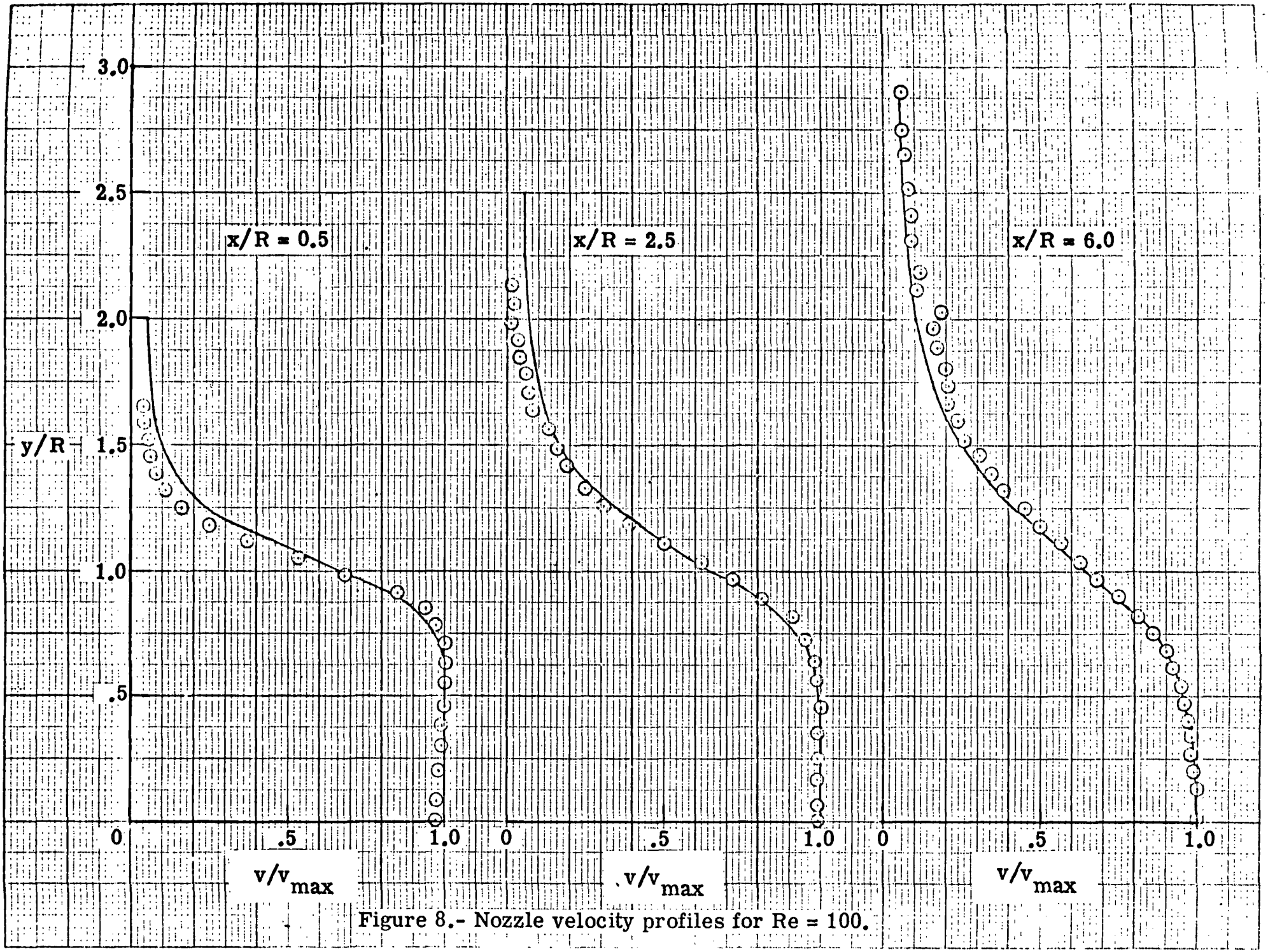

Figure 8.- Nozzle velocity profiles for Re = 100.

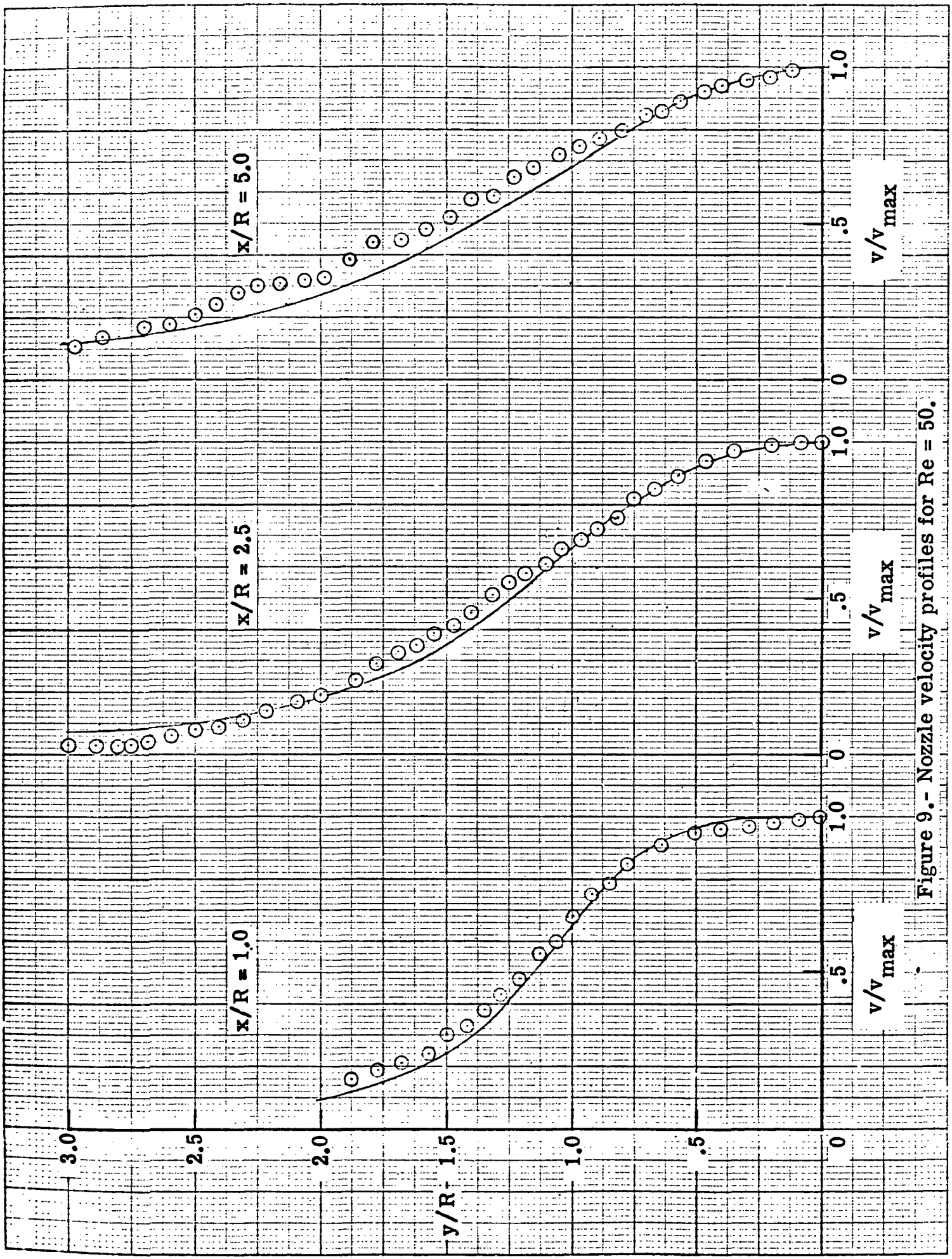

Figure 9.- Nozzle velocity profiles for Re = 50.

As mentioned earlier, the agreement between the measured and calculated results is very good with only a few exceptions. The agreement would probably be even better if it were not for two problems in calculating the flow field. The first problem is with the initial velocity profile which is used to start the flow field calculations. It was assumed that at the nozzle exit the velocity was uniform across the entire nozzle. At the edge of the nozzle, it was assumed that the velocity made a step change to the value associated with the background gas. However, the data indicate that the velocity was not quite uniform across the nozzle, especially at the higher Reynolds numbers. These errors enter the calculations and produce a large part of the discrepancies.

The other problem is in the value of velocity used for the background gas. The computer program which was used for these calculations is designed to handle either the flow field of a jet or the wake flow behind a body. However, wake flow calculations are its primary function. In wake calculations, it is very logical to nondimensionalize the velocity in the wake to the external flow velocity, u_e. However, this precludes calculating the flow field of a jet flowing into a fluid at rest since u_e would be zero and the nondimensional velocities would be infinite. This normally would not be a problem since u_e may be made arbitrarily small, and, as Pai [7] has shown, the solution is not overly sensitive to changes in u_e. However, for very low nozzle Reynolds numbers there is an additional problem. The numerical calculation step size is based on the Reynolds

number of the external flow. At low nozzle Reynolds numbers, small values of u_e produce prohibitively long run times. In this study, u_e was taken to be 5 percent of the jet velocity for all calculations. This produced reasonable run times without introducing excessively large errors in the calculated velocity profiles.

The primary effect of u_e is to change the jet spreading rate. This effect is shown in Figures 10 through 14. The 0.5 velocity radius (value of y/R at which $v/v_{max} = 0.5$) is plotted versus x/R for Reynolds numbers of 1000, 600, 200, 100, and 50. The 0.5 velocity radius is a measure of the jet width and its change in the downstream direction is a measure of the jet spreading rate. These figures show that the experimentally determined spreading rate is greater than that calculated using a value of u_e which is 5 percent of the jet velocity. This is also what one would expect intuitively.

At nozzle Reynolds numbers of 50 and 100, the nozzle velocity was 100 ft/sec rather than 200 ft/sec which was used for all the other tests conditions. In order to determine if this change had any affect on the results, flow field calculations were made for both 100 ft/sec and 200 ft/sec velocities at the same nozzle Reynolds number. The nondimensional velocity profiles were identical which indicates that the mixing and spreading of an incompressible jet is a function of only the Reynolds number.

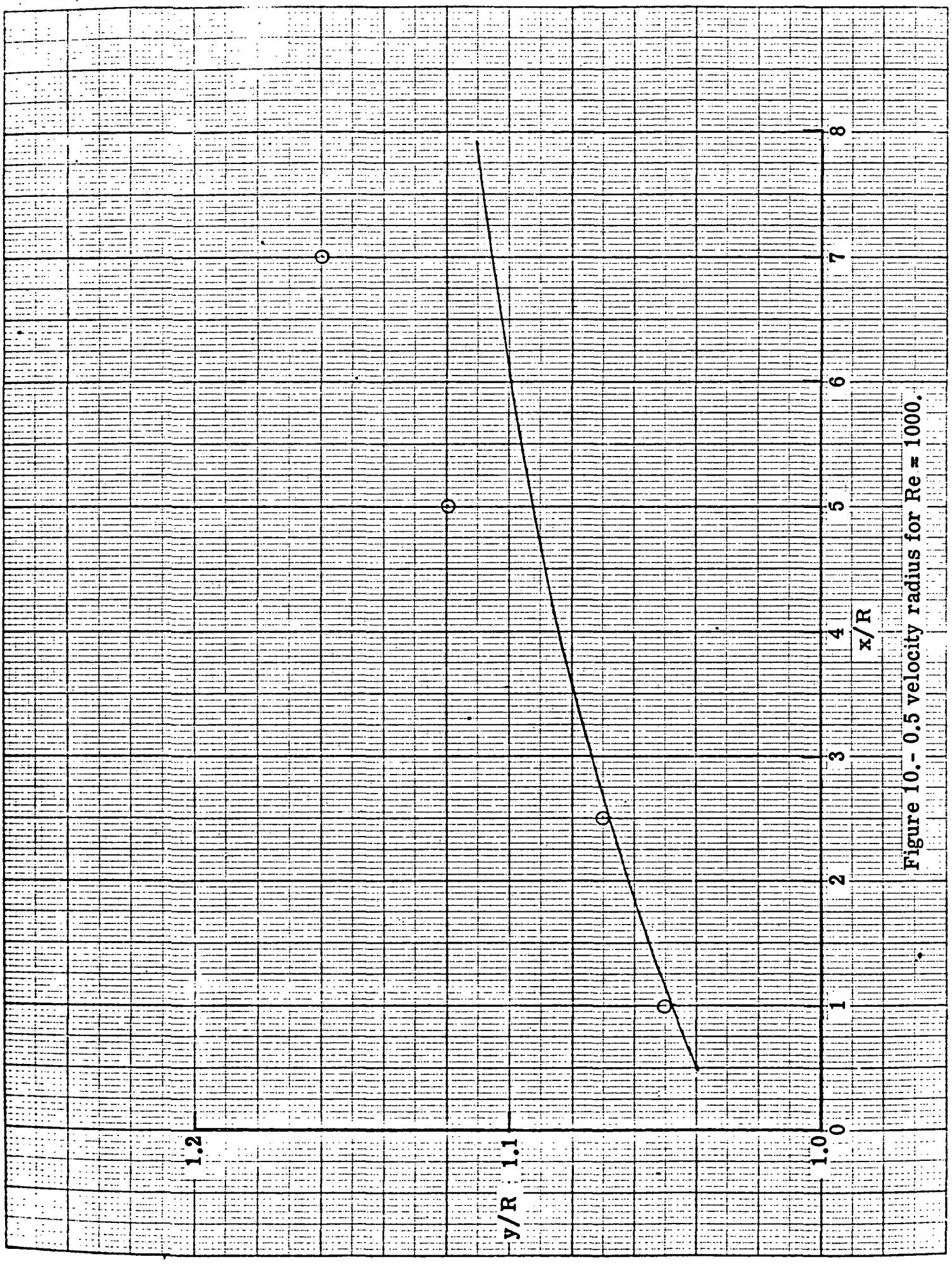

Figure 10.- 0.5 velocity radius for Re = 1000.

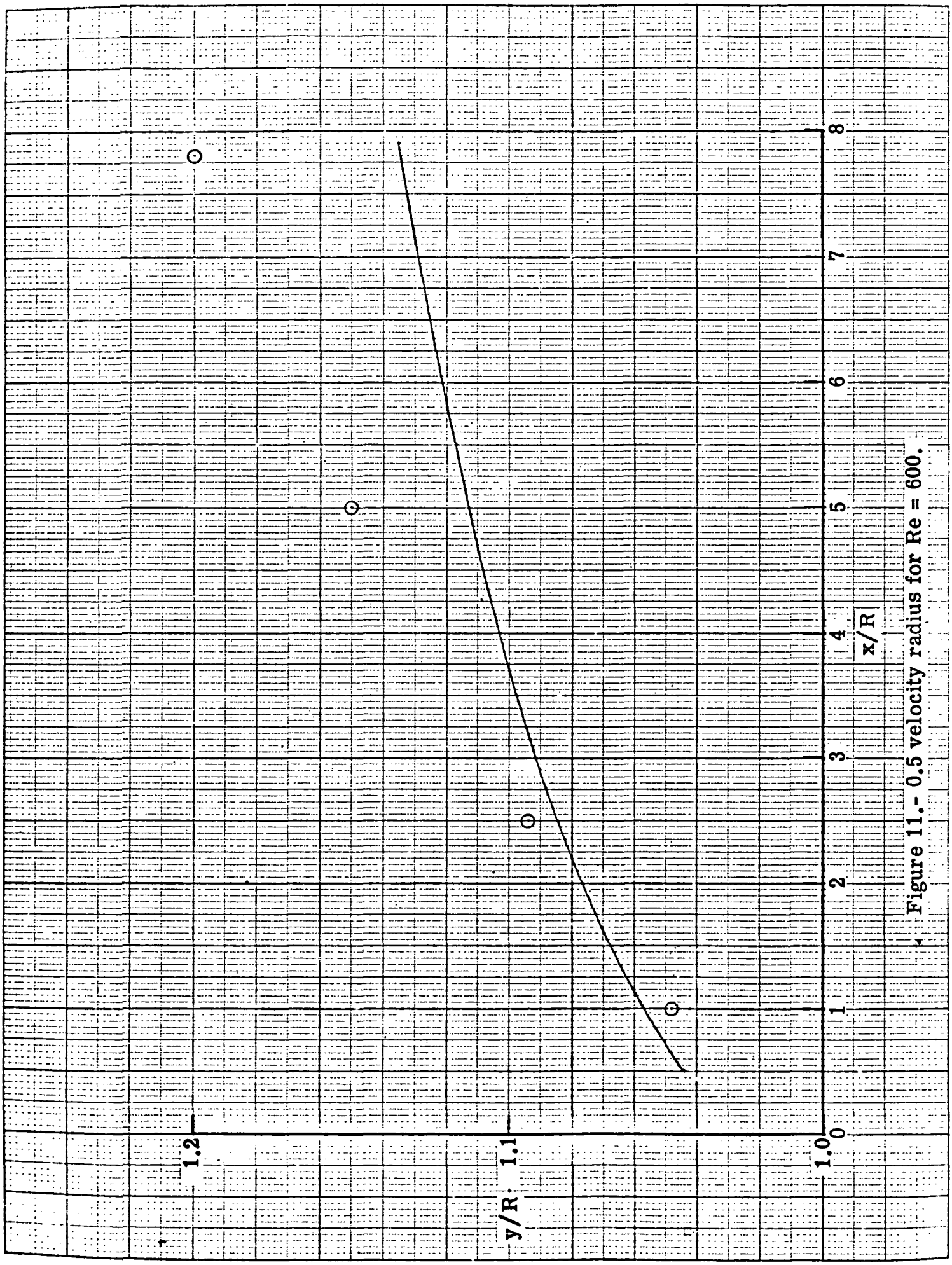

Figure 11.- 0.5 velocity radius for Re = 600.

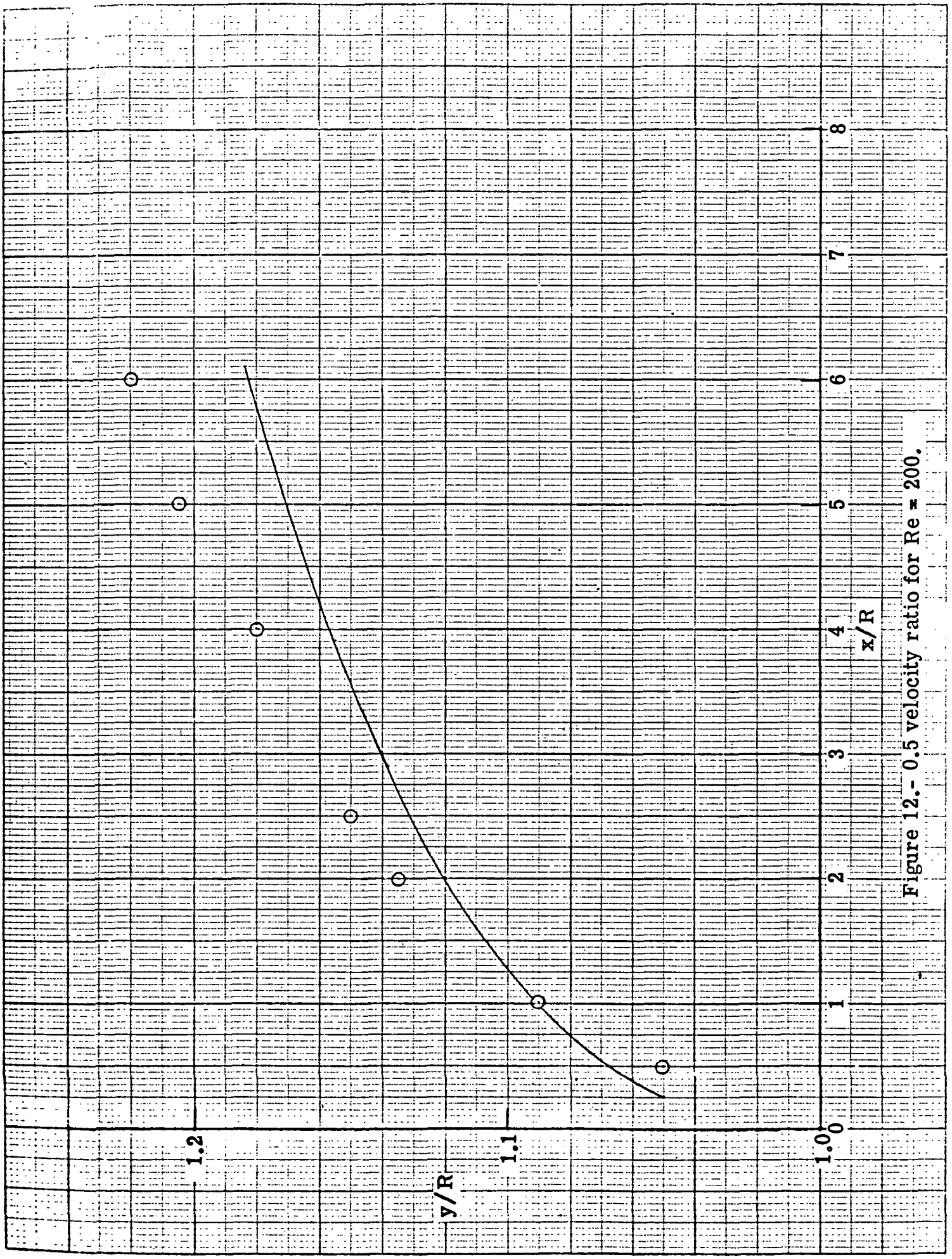

Figure 12.- 0.5 velocity ratio for Re = 200.

BOSTON, MASS. 02210
MADE IN U. S. A

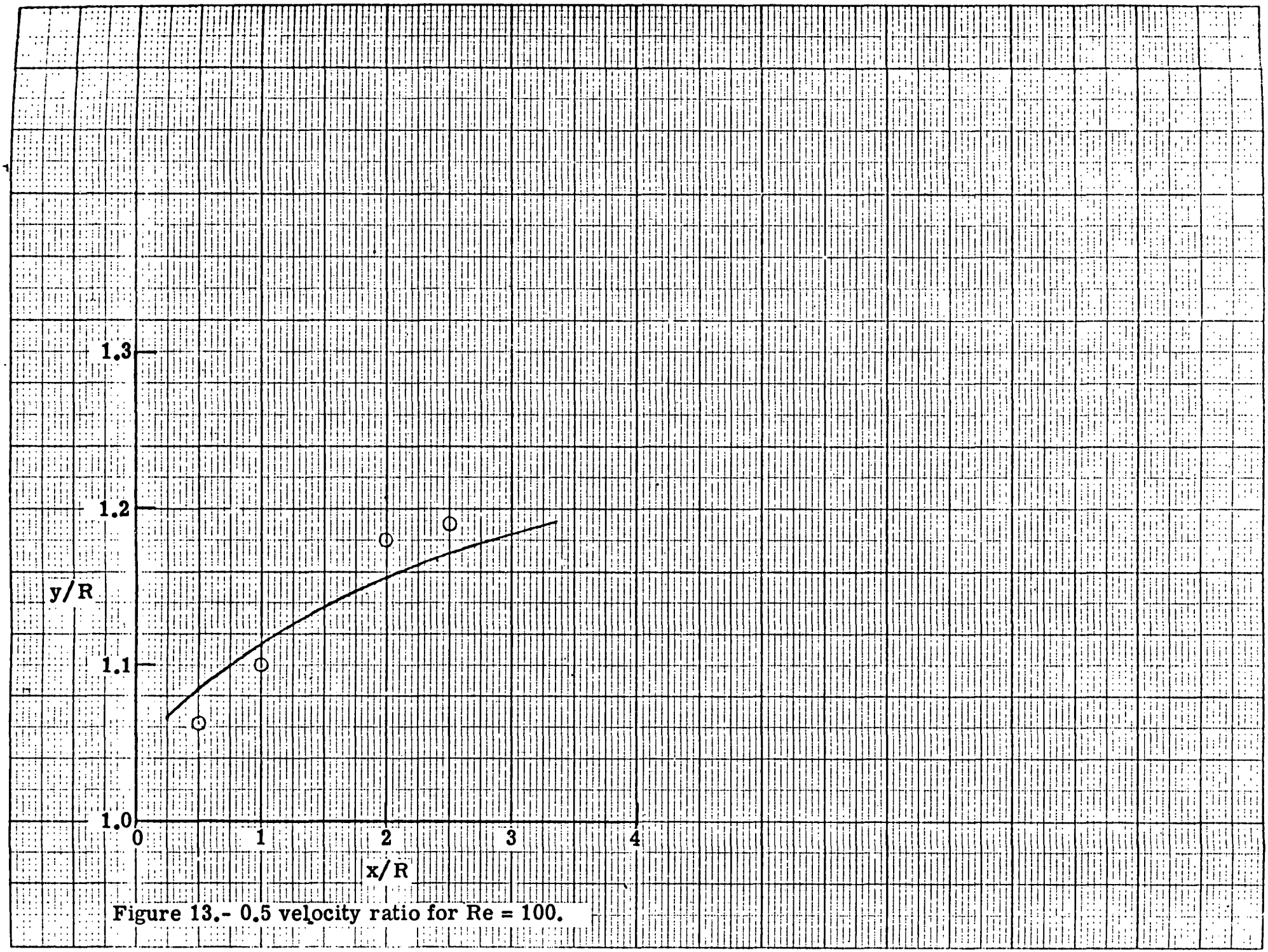

Figure 13.- 0.5 velocity ratio for Re = 100.

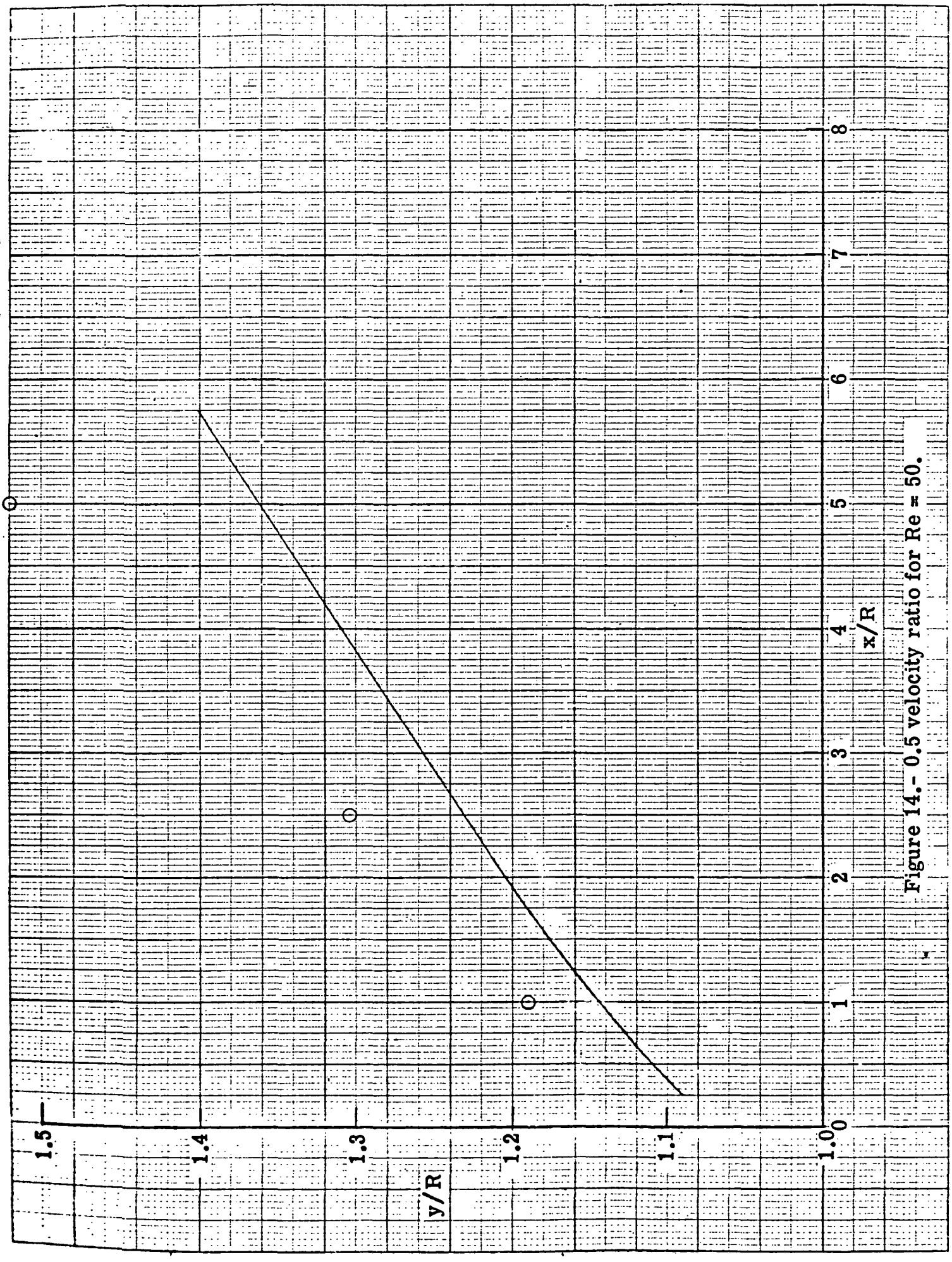

Figure 14.- 0.5 velocity ratio for Re = 50.

CONCLUSIONS

1. The porous plate nozzle produced a reasonably uniform velocity profile over a range of Reynolds numbers from 1000 down to 50. This contrasts with a conventional contoured nozzle which would have a large boundary layer at a Reynolds number of 1000 and would be completely filled with boundary layer at Reynolds numbers on the order of 200.

2. A conventional boundary layer type analysis was sufficient to accurately calculate the jet flow field for nozzle Reynolds numbers as low as 50.

3. The calculated mixing and spreading of an incompressible jet issuing into a medium at rest was a function of the Reynolds number only. Calculations at the same nozzle Reynolds number but different velocities produced essentially identical results.

REFERENCES

1. Stalder, J. R., "The Use of Low-Density Wind Tunnels in Aerodynamic Research", Rarefied Gas Dynamics, Vol. 3, Pergamon Press, 1960, pp. 1-20.

2. Sherman, F. S., "New Experiments on Impact-Pressure Interpretation in Supersonic and Subsonic Air Streams", NACA TN 2995, 1953.

3. Schaaf, S. A., "The Pitot Probe in Low-Density Flow", AGARD Report 525, January 1966.

4. Pao, Richard, H. F., Fluid Dynamics, Charles E. Merrill Books, Inc. 1967, p. 201.

5. Fox, H., Sinha, R., and Weinberger, L., "An Implicit Finite Difference Solution for Jet and Wake Problems", Astronautica Acta, Vol. 17, No. 3, 1972.

6. "Equations, Tables, and Charts for Compressible Flow", NACA TR 1135, 1953.

7. Pai, Shih - I, Fluid Dynamics of Jets, D. Van Nostrand Co., Inc. 1954, p. 82.